Figure S1

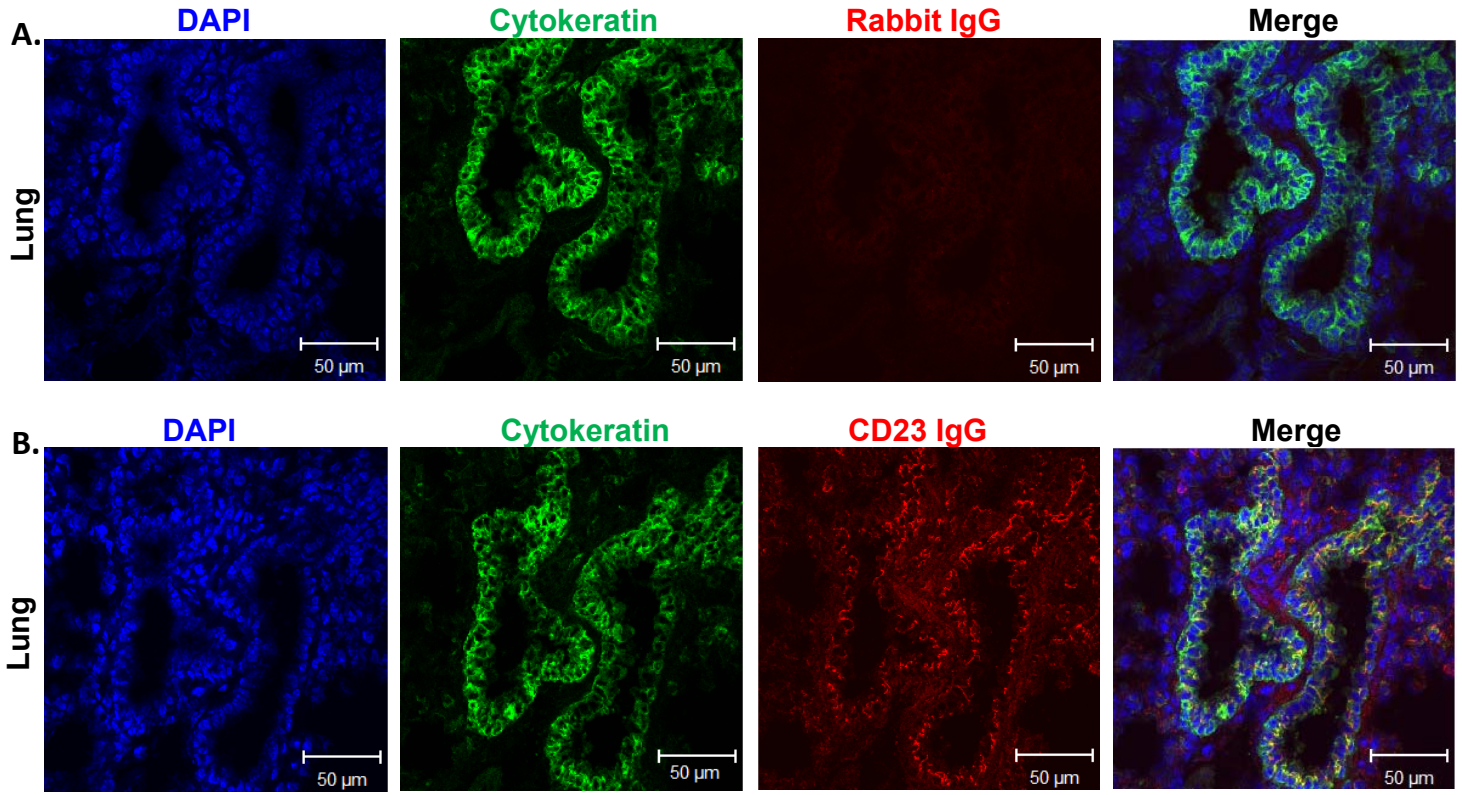
A.
DAPI
Cytokeratin
Rabbit IgG
Merge
Lung
50 μm
B.
DAPI
Cytokeratin
CD23 IgG
Merge
Lung
50 μm

Figure S1

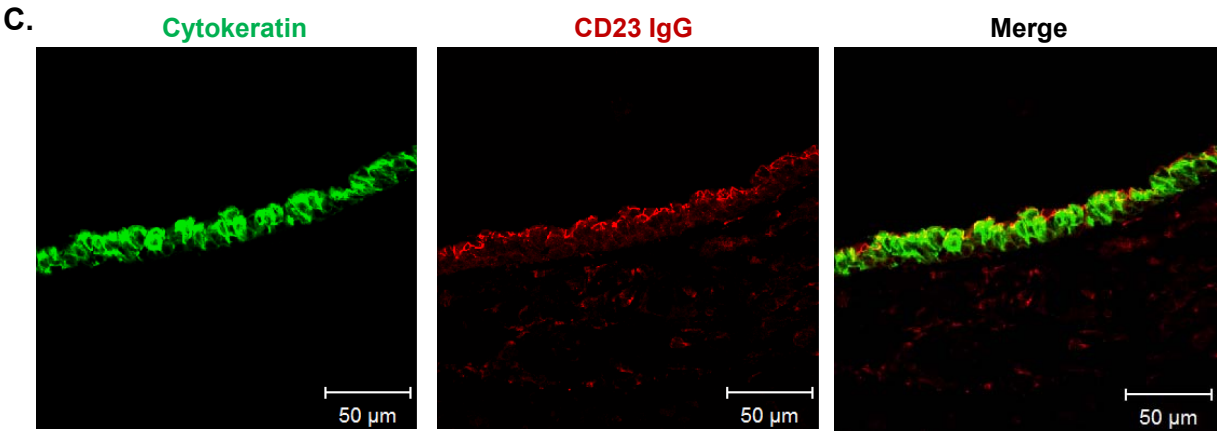

Figure S2.

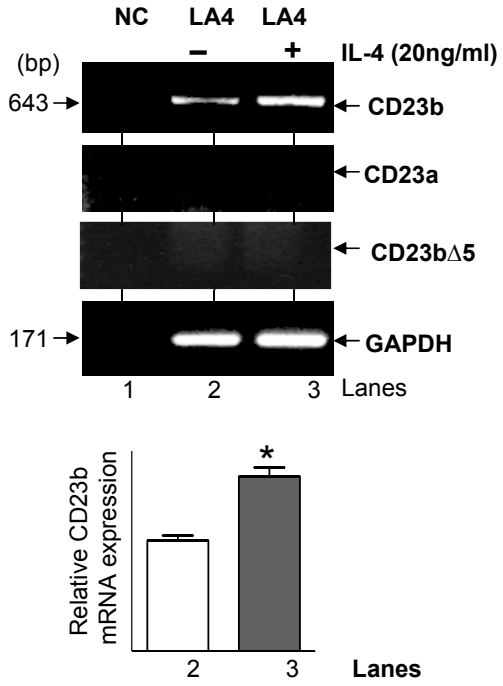
NC
LA4
LA4
–
+
IL-4 (20ng/ml)
(bp)
643
CD23b
CD23a
CD23bΔ5
171
GAPDH
1
2
3
Lanes
Relative CD23b mRNA expression
*
2
3
Lanes

Figure S3.

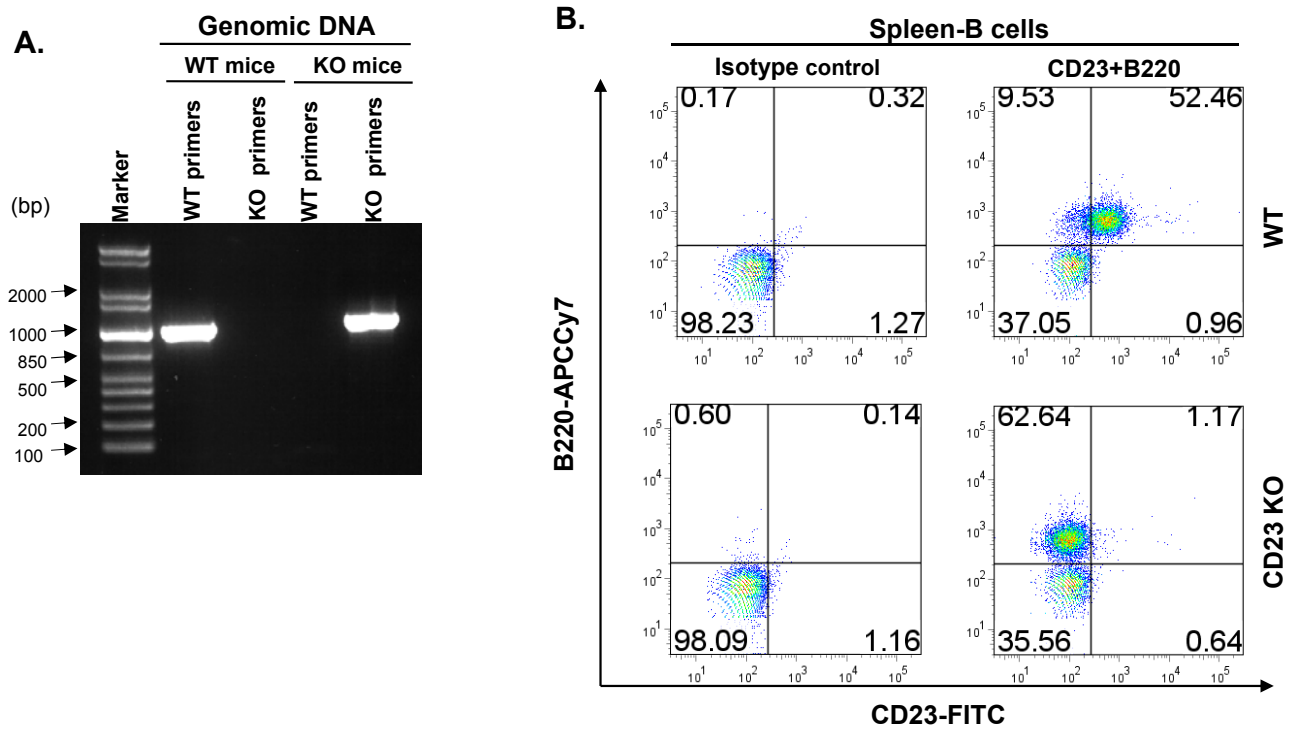
A.
Genomic DNA
WT mice
KO mice
Marker
WT primers
KO primers
WT primers
KO primers
(bp)
2000
1000
850
500
200
100
B.
Spleen-B cells
Isotype control
CD23+B220
0.17
0.32
98.23
1.27
9.53
52.46
37.05
0.96
0.60
0.14
98.09
1.16
62.64
1.17
35.56
0.64
WT
CD23 KO
B220-APCCy7
CD23-FITC

Figure S4.

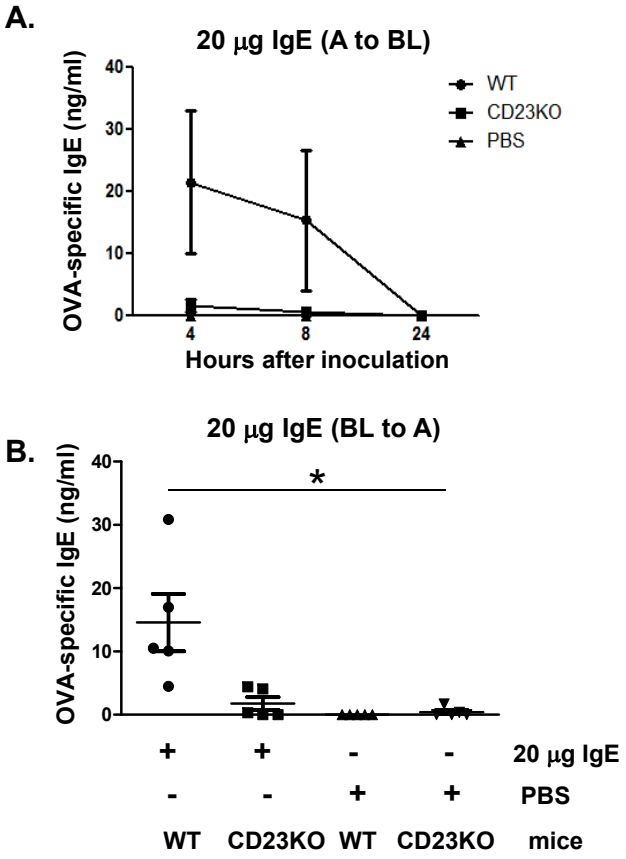
A.
20 μg IgE (A to BL)
OVA-specific IgE (ng/ml)
40
30
20
10
0
4
8
24
Hours after inoculation
WT
CD23KO
PBS
B.
20 μg IgE (BL to A)
OVA-specific IgE (ng/ml)
*
+ + - - 20 μg IgE
- - + + PBS
WT CD23KO WT CD23KO mice

Figure S5.

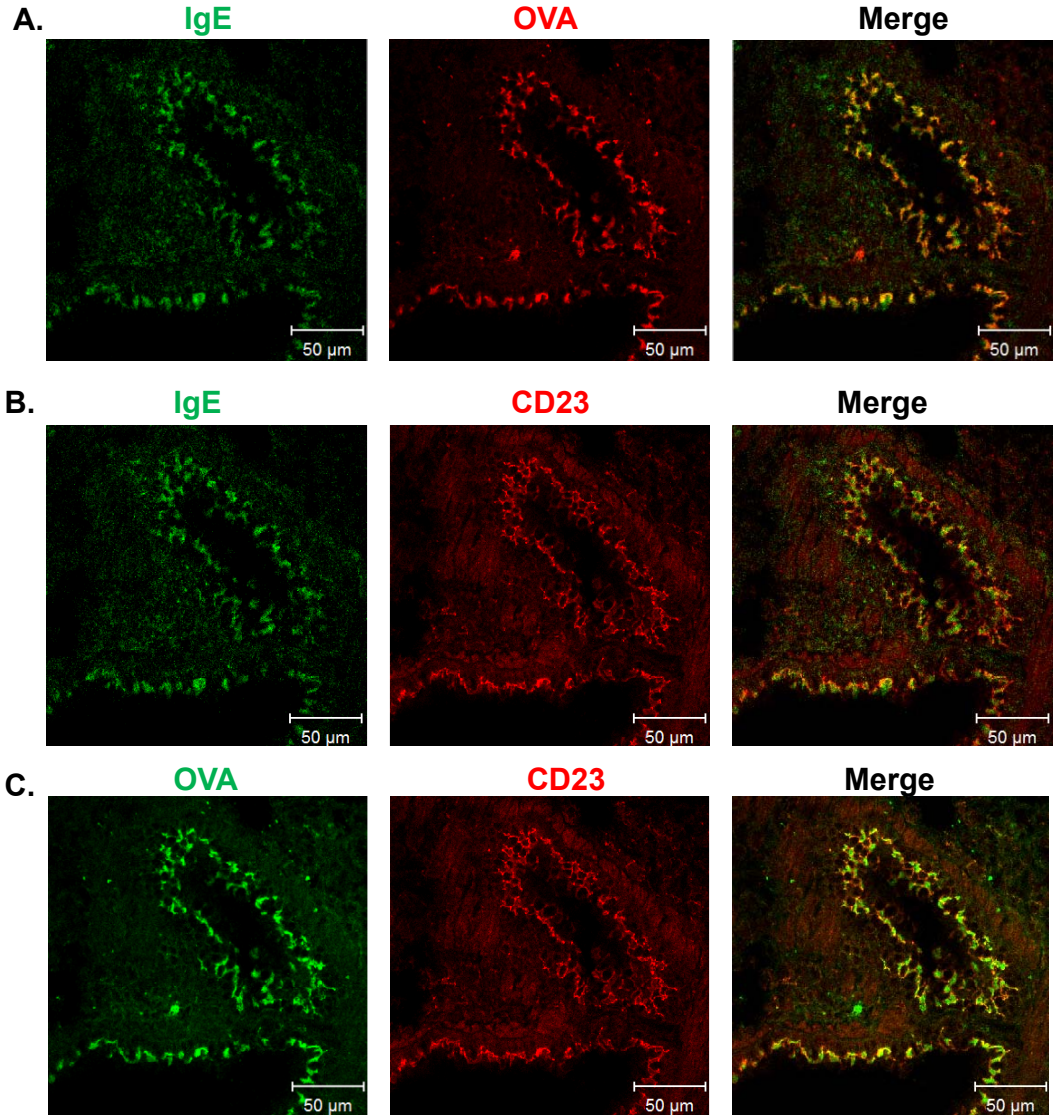

Figure S5.

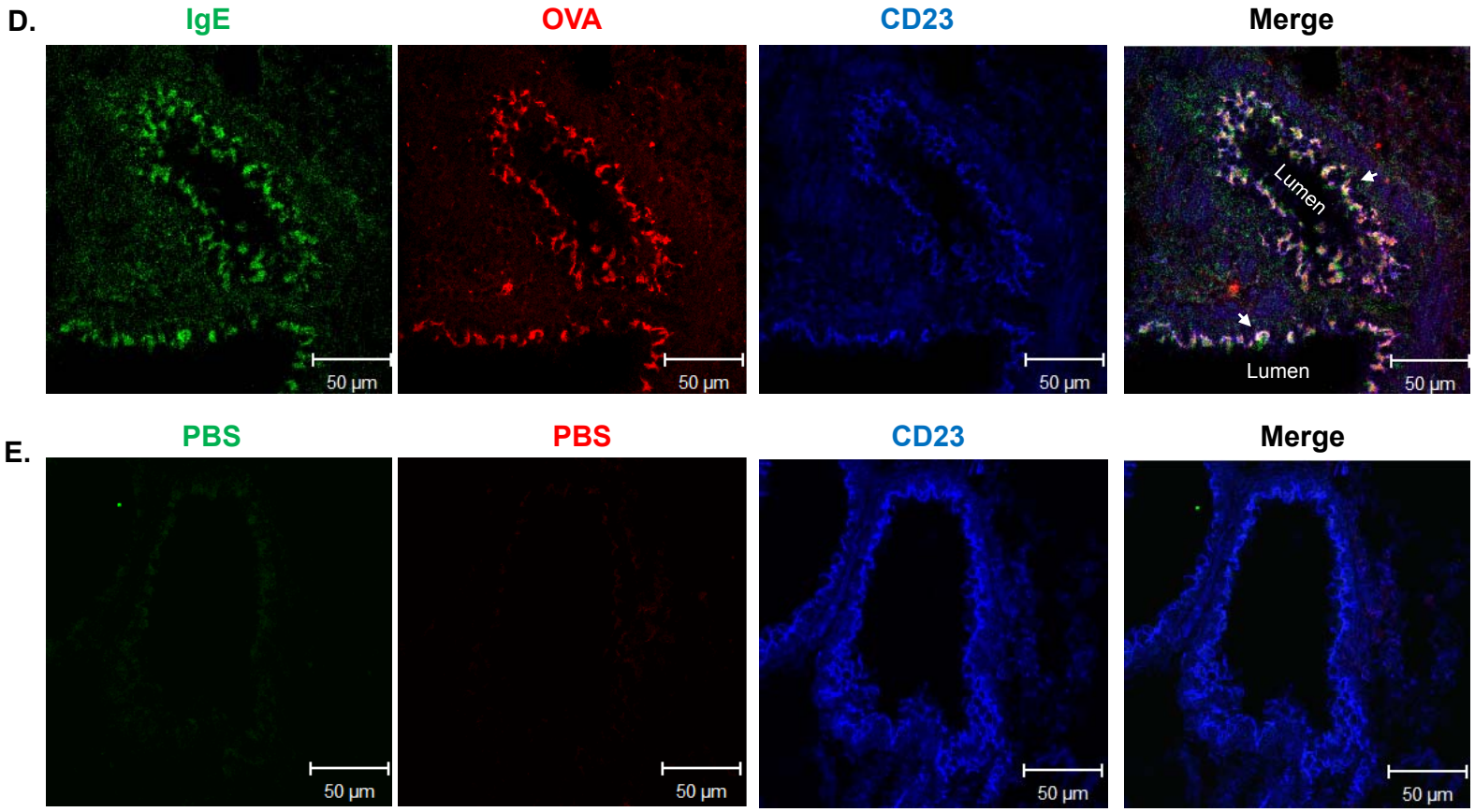
D.
IgE
OVA
CD23
Merge
50 μm
50 μm
50 μm
Lumen
Lumen
50 μm
E.
PBS
PBS
CD23
Merge
50 μm
50 μm
50 μm
50 μm

Figure S6.

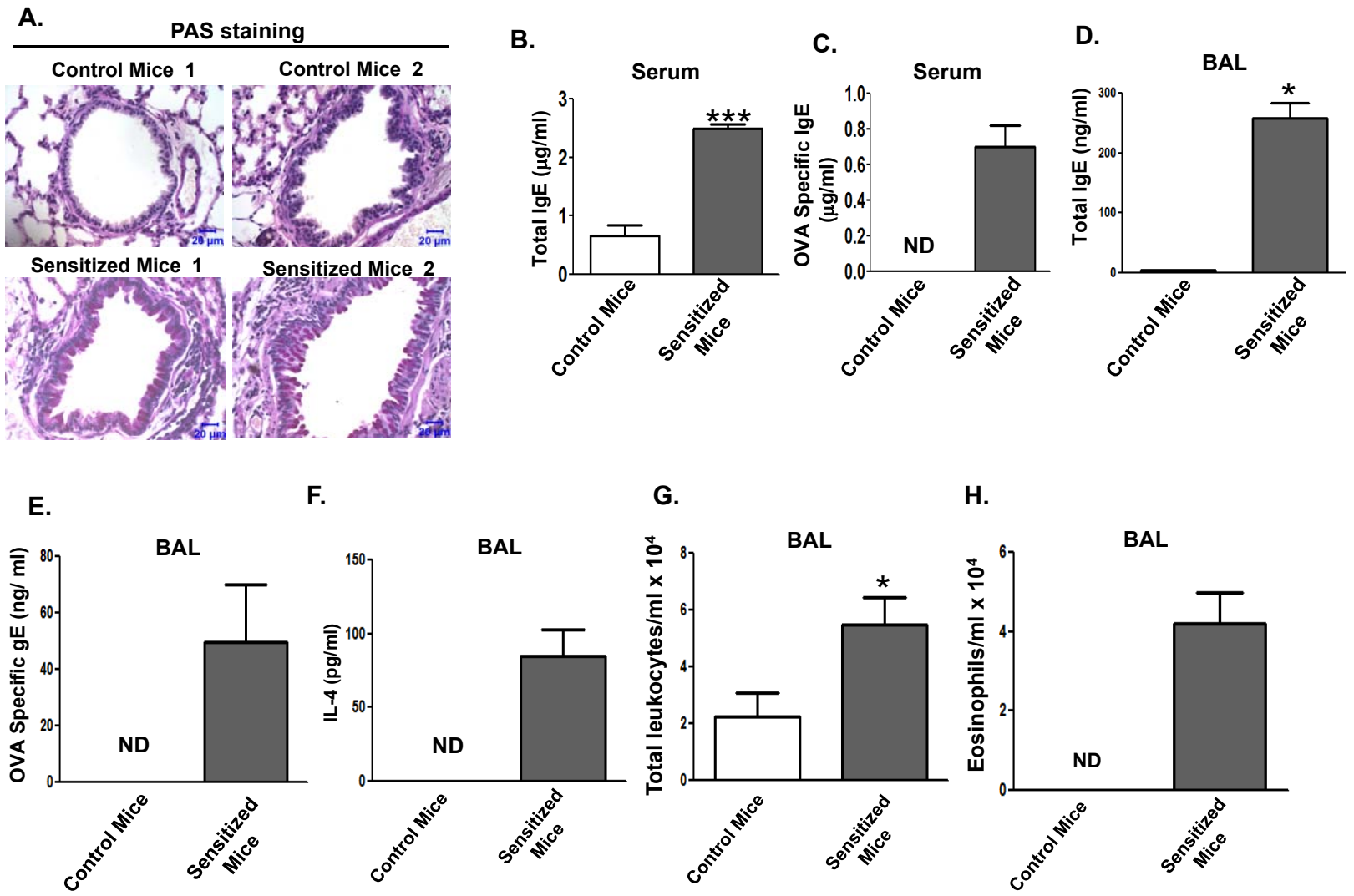
A.
PAS staining
Control Mice 1
Control Mice 2
Sensitized Mice 1
Sensitized Mice 2
B.
Serum
Total IgE (µg/ml)
***
Control Mice
Sensitized Mice
C.
Serum
OVA Specific IgE (µg/ml)
ND
Control Mice
Sensitized Mice
D.
BAL
Total IgE (ng/ml)
*
Control Mice
Sensitized Mice
E.
BAL
OVA Specific gE (ng/ ml)
ND
Control Mice
Sensitized Mice
F.
BAL
IL-4 (pg/ml)
ND
Control Mice
Sensitized Mice
G.
BAL
Total leukocytes/ml x 10⁴
*
Control Mice
Sensitized Mice
H.
BAL
Eosinophils/ml x 10⁴
ND
Control Mice
Sensitized Mice

Figure S7.

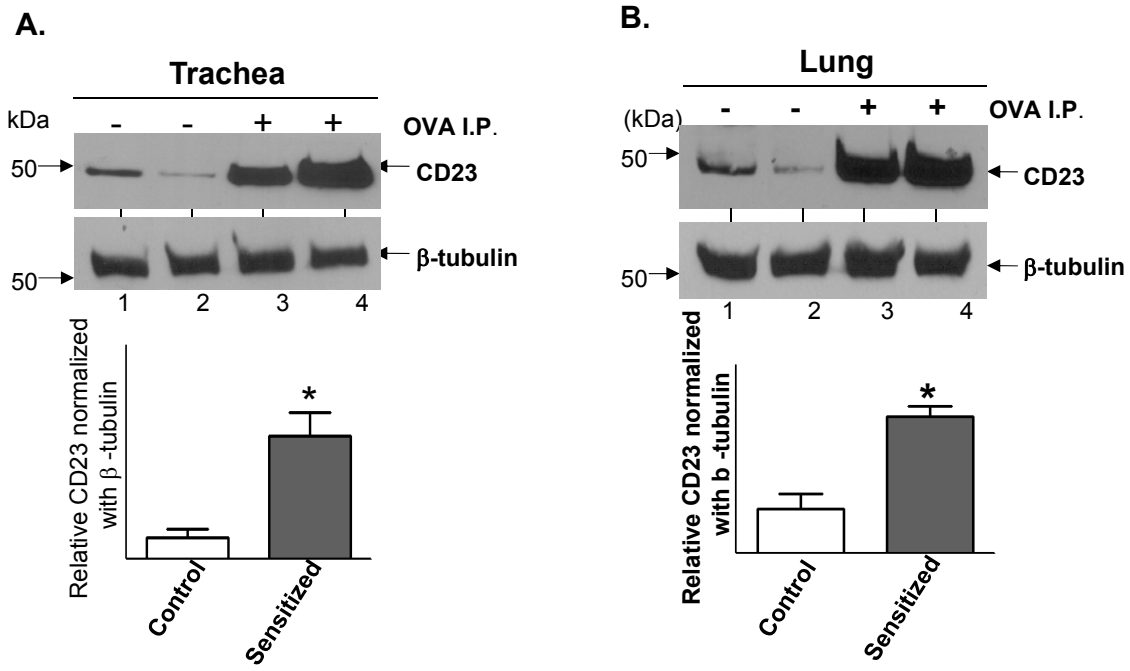
A.
Trachea
kDa
- - + +
OVA I.P.
50
CD23
50
β-tubulin
1 2 3 4
Relative CD23 normalized with β -tubulin
*
Control
Sensitized
B.
Lung
(kDa)
- - + +
OVA I.P.
50
CD23
50
β-tubulin
1 2 3 4
Relative CD23 normalized with b -tubulin
*
Control
Sensitized

Figure S8.

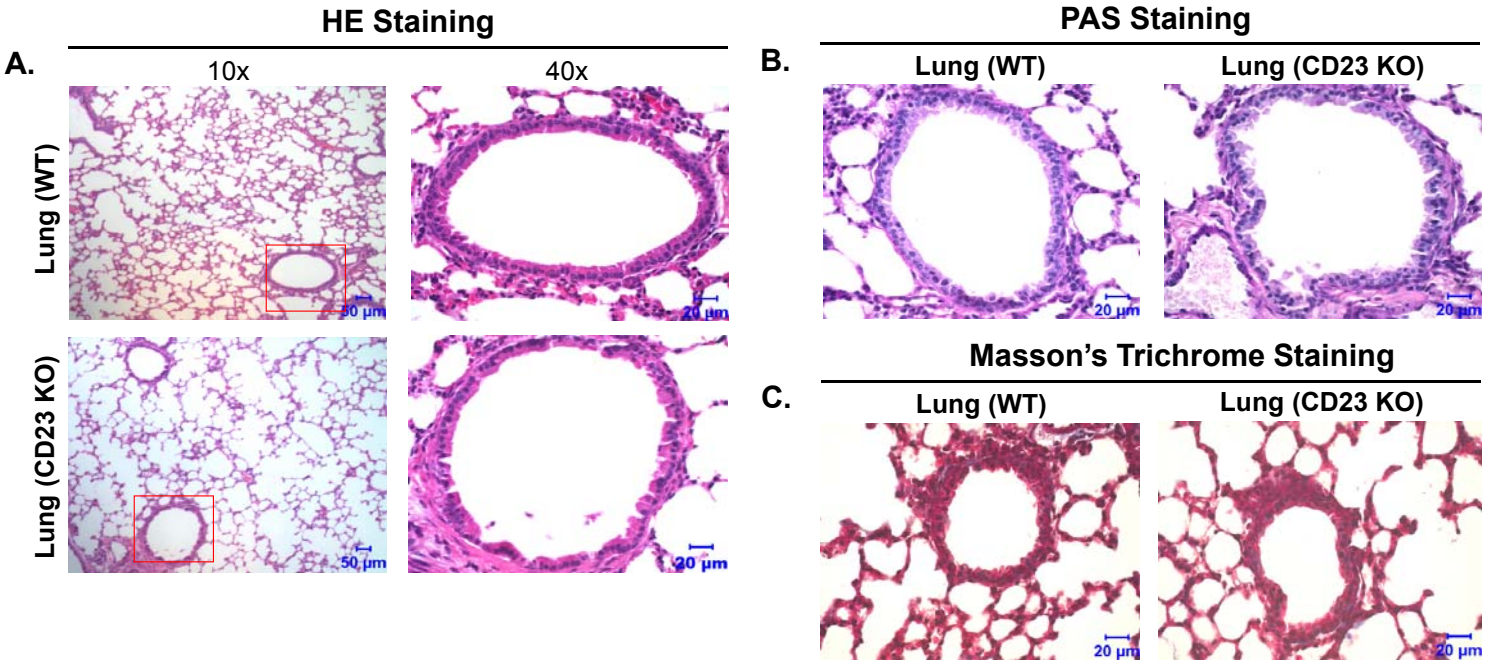
A.
HE Staining
10x
40x
Lung (WT)
Lung (CD23 KO)
50 μm
20 μm
B.
PAS Staining
Lung (WT)
Lung (CD23 KO)
20 μm
C.
Masson's Trichrome Staining
Lung (WT)
Lung (CD23 KO)
20 μm

Figure S9.

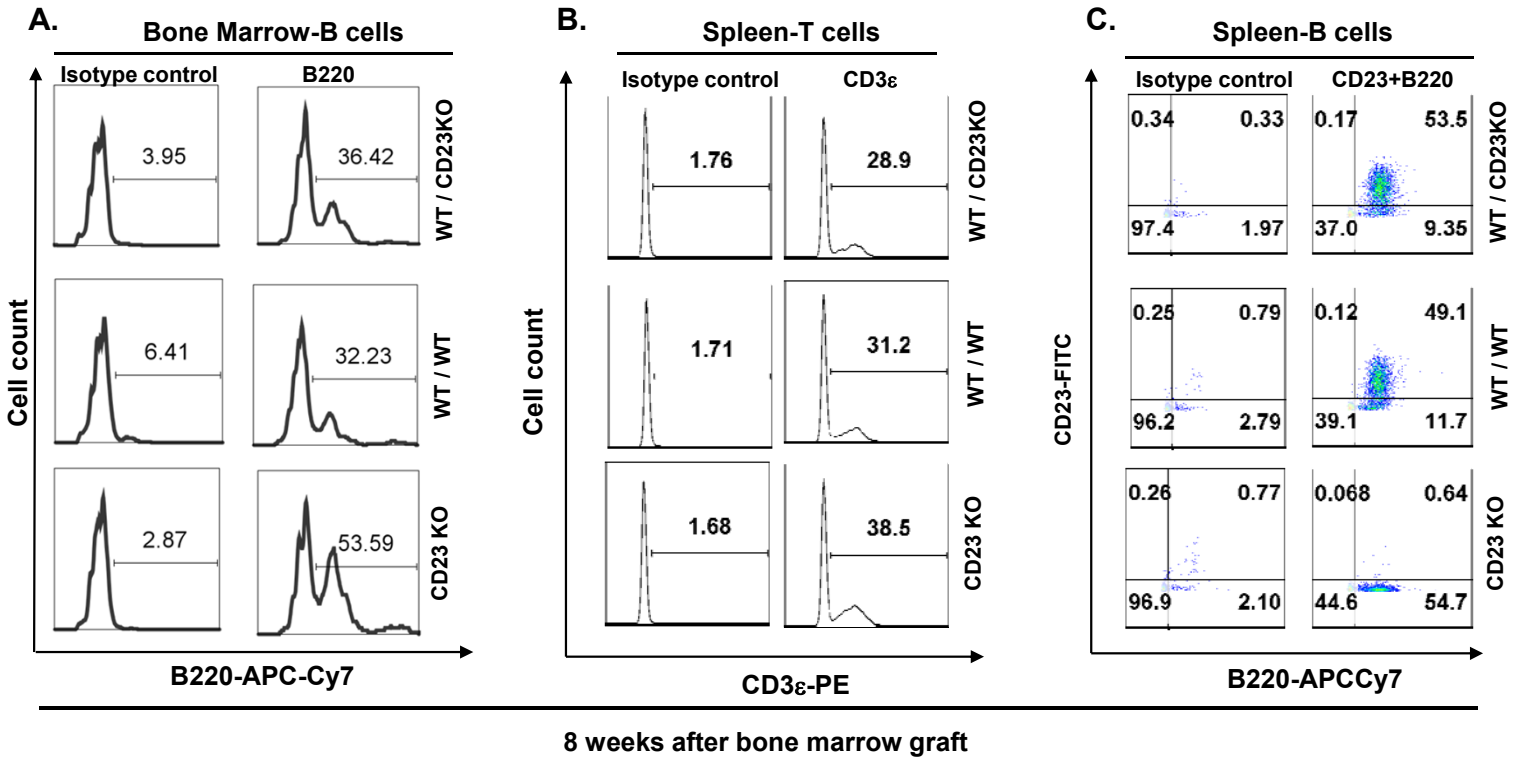
A.
Bone Marrow-B cells
Isotype control
B220
3.95
36.42
6.41
32.23
2.87
53.59
WT / CD23KO
WT / WT
CD23 KO
Cell count
B220-APC-Cy7
B.
Spleen-T cells
Isotype control
CD3ε
1.76
28.9
1.71
31.2
1.68
38.5
WT / CD23KO
WT / WT
CD23 KO
Cell count
CD3ε-PE
C.
Spleen-B cells
Isotype control
CD23+B220
0.34
0.33
97.4
1.97
0.17
53.5
37.0
9.35
0.25
0.79
96.2
2.79
0.12
49.1
39.1
11.7
0.26
0.77
96.9
2.10
0.068
0.64
44.6
54.7
WT / CD23KO
WT / WT
CD23 KO
CD23-FITC
B220-APCCy7
8 weeks after bone marrow graft

Figure S9

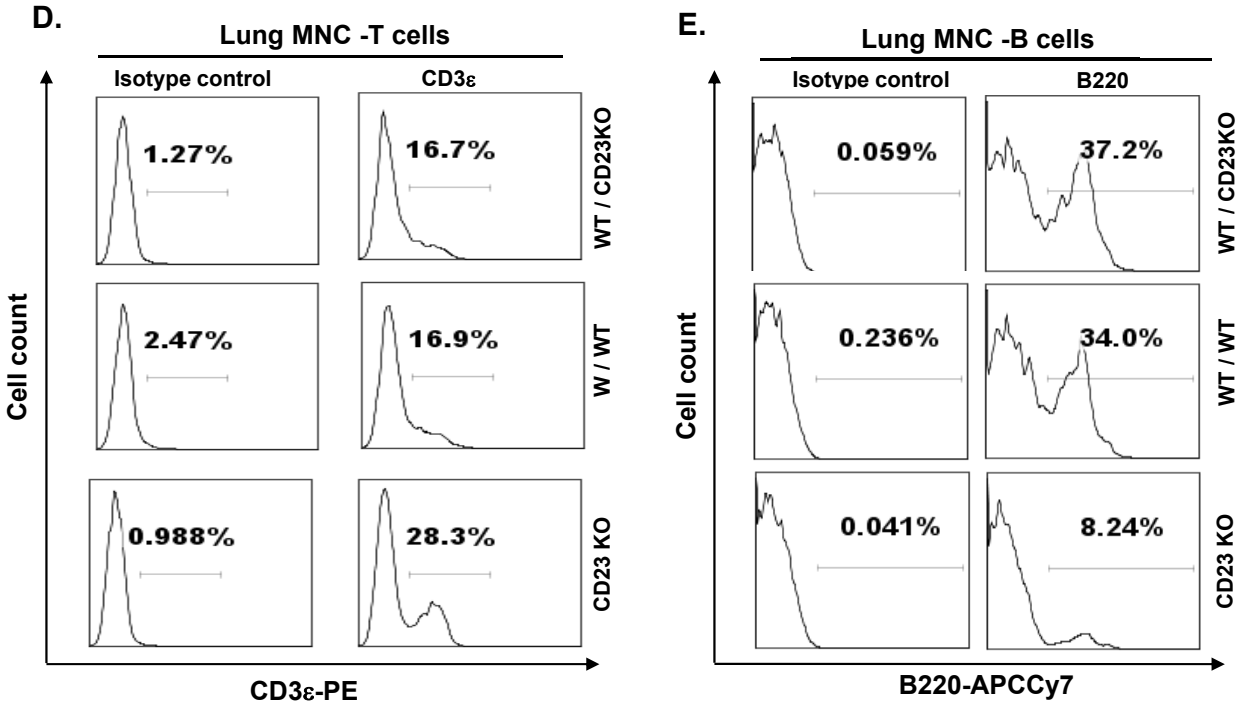
D.
Lung MNC -T cells
Isotype control
CD3ε
1.27%
16.7%
2.47%
16.9%
0.988%
28.3%
WT / CD23KO
W / WT
CD23 KO
Cell count
CD3ε-PE
E.
Lung MNC -B cells
Isotype control
B220
0.059%
37.2%
0.236%
34.0%
0.041%
8.24%
WT / CD23KO
WT / WT
CD23 KO
Cell count
B220-APCCy7

Figure S10

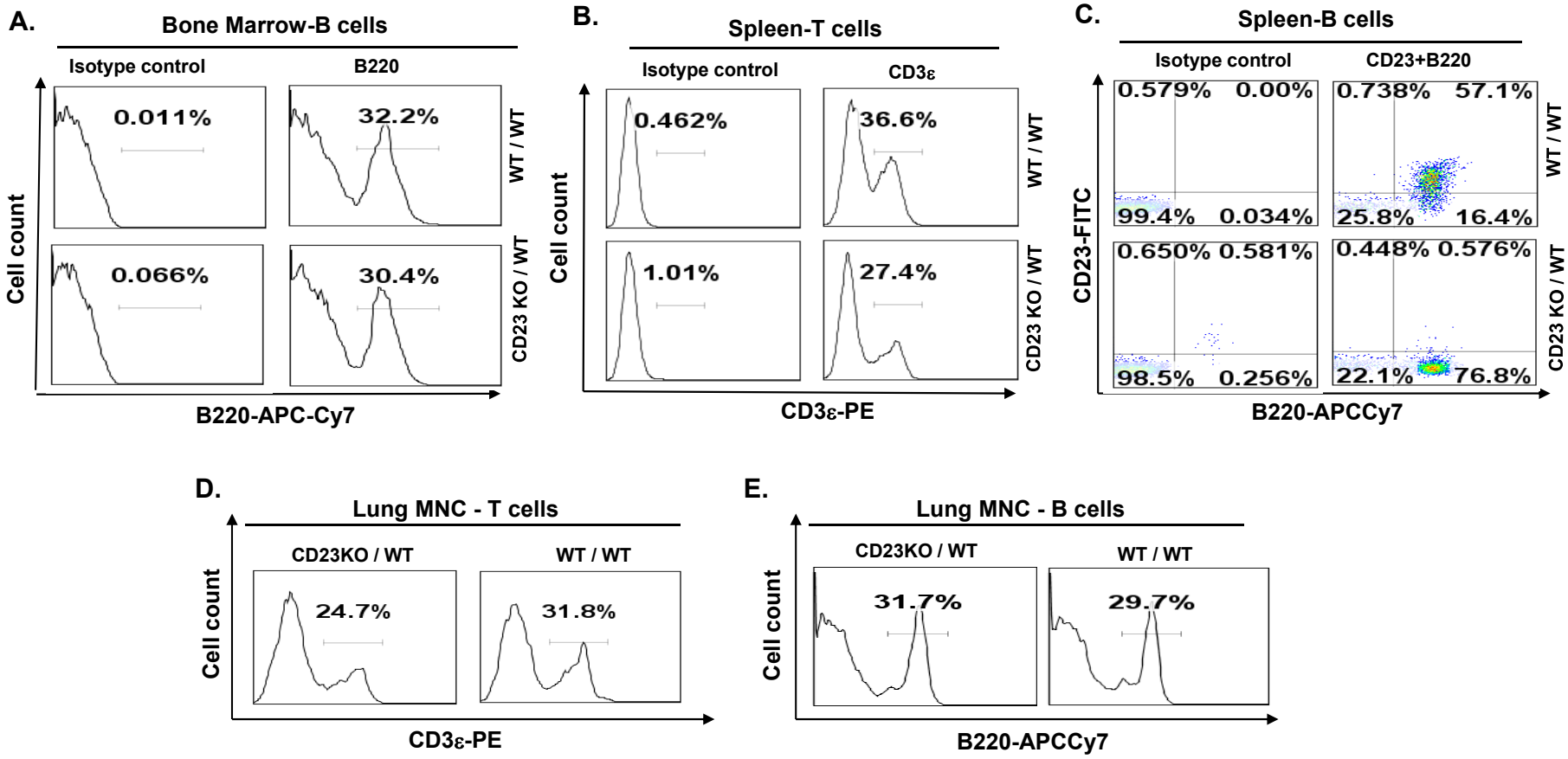
A.
Bone Marrow-B cells
Isotype control
B220
0.011%
32.2%
0.066%
30.4%
WT / WT
CD23 KO / WT
Cell count
B220-APC-Cy7
B.
Spleen-T cells
Isotype control
CD3ε
0.462%
36.6%
1.01%
27.4%
WT / WT
CD23 KO / WT
Cell count
CD3ε-PE
C.
Spleen-B cells
Isotype control
CD23+B220
0.579% 0.00%
99.4% 0.034%
0.738% 57.1%
25.8% 16.4%
0.650% 0.581%
98.5% 0.256%
0.448% 0.576%
22.1% 76.8%
WT / WT
CD23 KO / WT
CD23-FITC
B220-APCCy7
D.
Lung MNC - T cells
CD23KO / WT
WT / WT
24.7%
31.8%
Cell count
CD3ε-PE
E.
Lung MNC - B cells
CD23KO / WT
WT / WT
31.7%
29.7%
Cell count
B220-APCCy7

Figure S11.

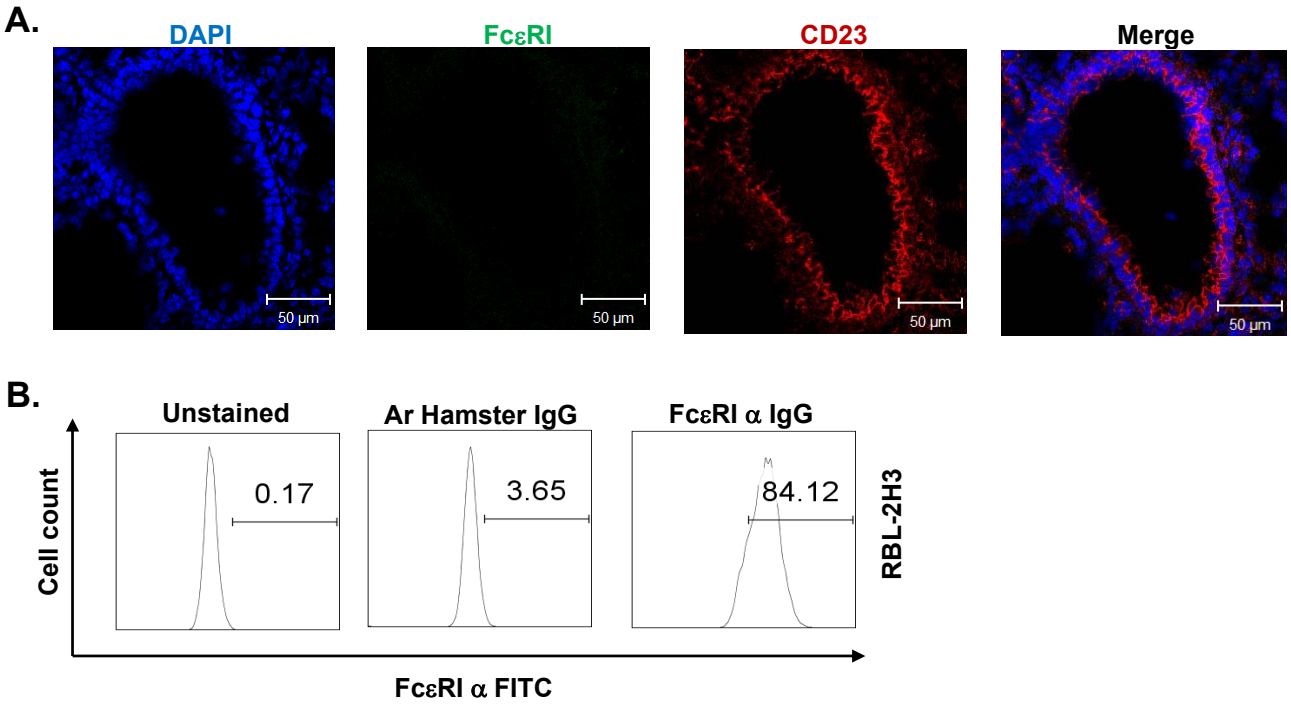
A.
DAPI
FcεRI
CD23
Merge
50 μm
50 μm
50 μm
50 μm
B.
Unstained
Ar Hamster IgG
FcεRI α IgG
0.17
3.65
84.12
Cell count
RBL-2H3
FcεRI α FITC

Figure S12.

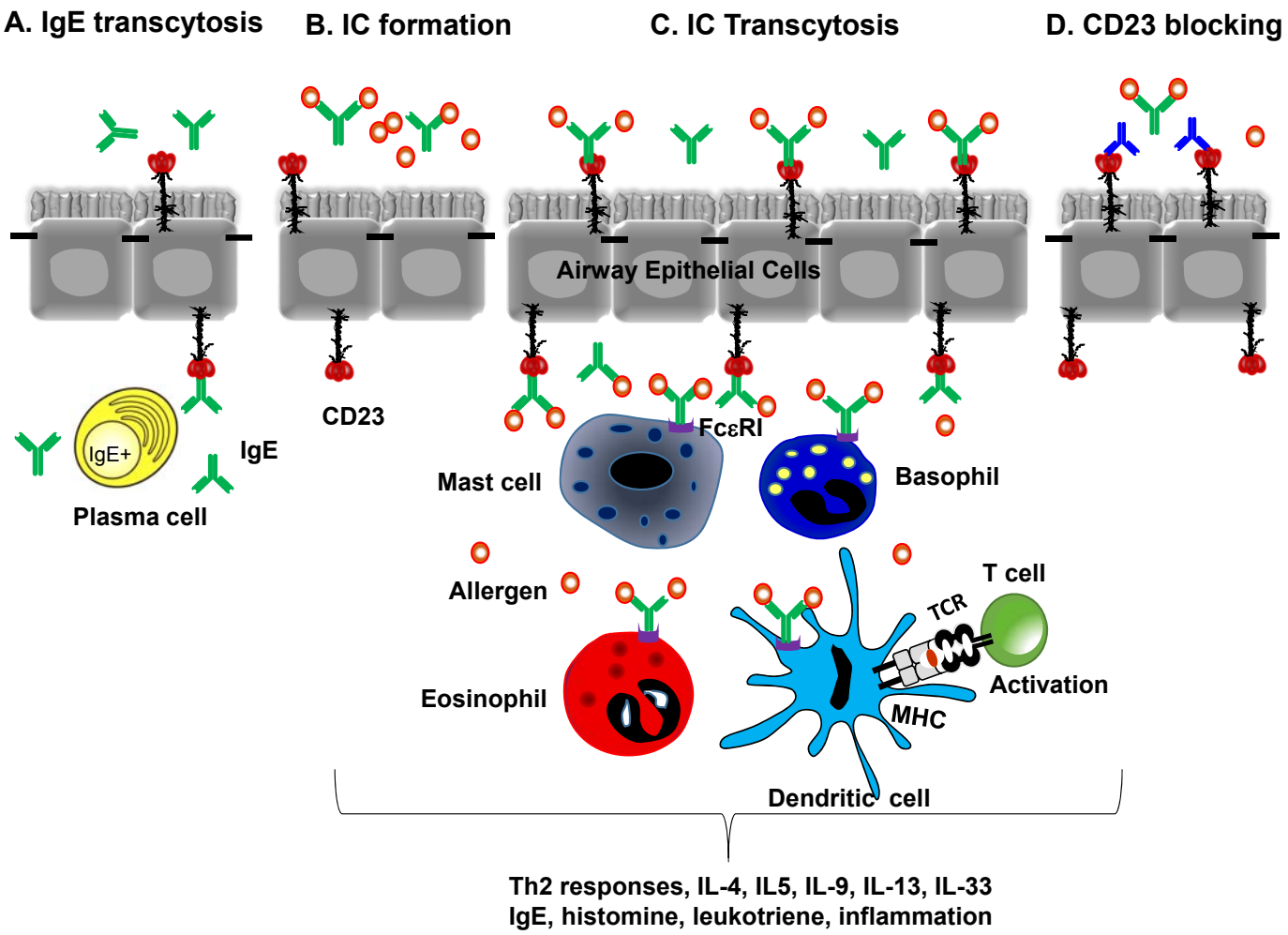
A. IgE transcytosis
B. IC formation
C. IC Transcytosis
D. CD23 blocking
Airway Epithelial Cells
IgE+
IgE
Plasma cell
CD23
FcεRI
Mast cell
Basophil
Allergen
T cell
TCR
Activation
Eosinophil
MHC
Dendritic cell
Th2 responses, IL-4, IL5, IL-9, IL-13, IL-33
IgE, histomine, leukotriene, inflammation

SUPPLEMENTARY MATERIALS

Fig S1. CD23 expression colocalized with the epithelial marker cytokeratin in mouse lung. The WT mouse lung (A+B) or trachea (C) was prepared in OCT medium and cryosectioned at 5 μm. The sections were fixed and permeabilized with ice-cold acetone and blocked with 10% NGS. The sections were incubated with rabbit anti-CD23 Ab or normal rabbit IgG, followed by staining with Alexa Flour 555-conjugated goat anti-rabbit Ab and FITC-conjugated mouse anti pan-cytokeratin Ab. The nucleus was stained with DAPI. Images were captured using Zeiss LSM510 confocal microscope. Samples were visualized under same contrast and brightness setting.

Fig S2. CD23b-specific mRNA is expressed in LA4 mouse lung epithelial cells. TRIzol reagent was used to extract total RNA from untreated-LA4 lung epithelial cells (lane 2), IL-4 (20 ng/ml) treated LA4 cells (lane 3), and a negative control without the addition of mRNA template (lane 1). RT-PCR was performed to amplify CD23a, CD23b, CD23bΔ5, and GAPDH using gene-specific primers as described in the Materials and Methods. Amplified PCR products were electrophoresed in 1.5% agarose gels and stained with ethidium bromide. The arrow indicates amplification products for mouse CD23 and GAPDH. Densitometry of CD23b band intensities normalized to GAPDH is presented in the bottom panel. *$P<0.05$.

Fig S3. CD23 KO mice were verified by PCR amplification of tail DNA and flow cytometric analysis of CD23 expression in spleenic B cells in comparison with that of WT mice.

Fig S4. Airway transcytosis of mouse IgE in wild type (WT) or CD23 KO mice. A: OVA-specific IgE (20 μg) was i.n. inoculated into either WT or CD23 KO mice for 5 min. Sterile PBS

was used as a control. Sera were collected at indicated time points. **B**: OVA-specific IgE (20 μg) or sterile PBS was i.p. inoculated into either WT or CD23 KO mice. BAL fluid was collected 8 h after injection. OVA-specific IgE was measured in the sera or BAL fluid by ELISA. A: Apical; BL: Basolateral. *P<0.05.

Fig S5. Colocalization of CD23 and ICs in the lung. The OVA-IgE ICs or PBS was i.n. inoculated into anaesthetized mice. Mice were sacrificed and 20 min later, the lung tissue was prepared in OCT medium and cryosectioned at 5 μm. Frozen sections were fixed and permeabilized with ice-cold acetone and blocked with 10% NGS. Sections were incubated with rabbit anti-CD23 Ab or mouse anti-chicken OVA Ab followed by staining with Alexa fluor 633-conjugated goat anti-rabbit Ab, Alexa fluor 555-conjugated goat anti-mouse Ab, and FITC conjugated goat anti-mouse IgE Ab. Nuclei were stained with DAPI and imaged using a Zeiss LSM510 confocal microscope. Samples were visualized under constant contrast and brightness settings. A pair-wise co-localization of CD23 (red) with either IgE (green) or OVA (green) produces the yellow in the merged picture. Co-localization of mouse CD23 (blue), IgE (green), and OVA (red) appears as white.

Fig S6. Mouse allergy model. WT mice were i.p. sensitized with 100 μg OVA dissolved in PBS plus 4 mg alum at day 0 and were then given an i.p. injection of 100 μg OVA dissolved in PBS on days 7 and 14. On day 21, 22, and 23 the mice were challenged with nebulized 1 % OVA for 30 min. Control mice were sensitized and challenged with PBS. Mice were sacrificed 24 h after the last aerosol challenge and lung tissues were formalin fixed and embedded in paraffin. Lung sections were stained with PAS (A). Serum and BAL fluids from either control or sensitized

mice were collected 24 h after the last aerosol challenge. Total IgE (B+D), OVA-specific IgE (C+E), and IL-4 (F) contents in either BAL or serum were measured by ELISA. The number of total leukocytes (G) or eosinophils (H) in the BAL fluid was counted using a hemocytometer and giemsa-stained cytospin. ND, not detected. *P<0.05; ***P<0.001.

Fig S7. Sensitization augments CD23 expression. (**A**) - (**B**). Mice were sensitized with OVA or left untreated. Epithelial cells from lung and trachea of naive and sensitized mice were isolated seven days after the last OVA sensitization as described in the Materials and Methods. Cell lysates (50 μg) from normal trachea or lung (lanes 1 & 2) and sensitized trachea or lung (lanes 3 & 4) were subjected to 12 % SDS-PAGE gel electrophoresis under reducing conditions. The separated proteins were transferred onto nitrocellulose membranes, blocked and blotted with rat anti-mouse CD23 Ab (B3B4) or with murine anti-β-tubulin Ab. Blots were washed and further incubated with HRP-conjugated rabbit anti-rat IgG Ab or HRP-conjugated rabbit anti-mouse Ab and the proteins were visualized using ECL. Arrows indicate CD23 and β-tubulin. Densitometry of CD23 band intensities normalized to the β-tubulin band intensities are presented in the bottom panel. *P<0.05

Fig S8. Histological lung sections reveal normal structures. Lung sections obtained from either WT or CD23 KO mice were stained with H.E., PAS, and Masson's trichrome staining. There were no significantly detectable differences in lung structure, goblet-cell hyperplasia, or peribronchial fibrosis between CD23KO and WT mice.

Fig S9. Representative flow cytometric analyses of immune cells after irradiation and repopulation in chimeric mice. WT and CD23 KO mice were irradiated and repopulated with WT bone marrow cells as described in the Materials and Methods. $B220^+$ B cells in the bone marrow, $CD23^+$ $B220^+$ B cells and $CD3\varepsilon^+$ T cells in the spleen, and lung mononuclear cells were analyzed at 8 weeks after bone marrow transplantation. Values are the percentages of B cells or T cells among gated cells.

Fig S10. Flow cytometric analysis of immune cells in irradiated mice. WT mice were irradiated and repopulated with CD23KO bone marrow cells as described in the Materials and Methods. $B220^+$ B cells in the bone marrow and lung mononuclear (MNC) cells, CD3 ε+ T cells and $CD23^+$ $B220^+$ B cells in the spleen were analyzed in the irradiated and bone marrow chimeric mice as indicated. Values are the percentages of B cells or T cells among gated cells.

Fig S11. FcεRI α chain was not expressed in mouse lung epithelial cells. A. WT mouse lung (top panel) was prepared in OCT medium and cryosectioned at 5 μm. The sections were fixed and permeabilized with ice-cold acetone and blocked with 10% NGS. The sections were incubated with hamster anti-mouse FcεRI Ab or rabbit anti-mouse CD23 Ab, followed by staining with Alexa Fluor 555-conjugated goat anti-rabbit Ab and FITC-conjugated goat anti-armenian hamster Ab. Nucleui were stained with DAPI. Images were captured using a Zeiss LSM510 confocal microscope. Samples were visualized under consistent contrast and brightness settings. **B.** RBL-2H3 cells expressing the FcεRIα chain were used as positive control. RBL-2H3 cells were stained with hamster anti-mouse FcεRI Ab, followed by staining with FITC-conjugated goat anti-armenian hamster Ab (bottom right panel). RBL-2H3 cells were also

stained with control FITC-conjugated Armenian hamster IgG Ab (bottom middle panel). Values represent the percentage of cells expressing FcεRIα chain.

Fig. S12. Proposed model for role of CD23 in AECs during allergic inflammation. IgE from mucosal plasma cells or from the blood are transported by CD23 into the airway lumen (A) where they capture airborne allergens (B). Allergen–IgE immune complexes (ICs) are captured by CD23 on the luminal side of the airway epithelium and transported back into the mucosa where they bind to FcεRI on the surface of leukocytes and dendritic cells causing allergic inflammation and antigen presentation (C). When CD23-specific antibody binds CD23 on the luminal side of the epithelium, such transcytosis is blocked (D). Consequently, allergic inflammation in the airway is attenuated.